PAIR DISTRIBUTION FUNCTIONS ANALYSIS

VALERI PETKOV

Department of Physics, Central Michigan University, Mt. Pleasant, MI, USA

INTRODUCTION

The atomic-scale structure, that is, how atoms are arranged in space, is a fundamental material's property. Pair distribution functions (PDF)s analysis is a widely used technique for characterizing the atomic-scale structure of materials of limited structural coherence. It was first applied on liquids and glasses (Warren, 1934). Recently, it was extended to crystals with intrinsic disorder (Egami and Billinge, 2003) and nanosized particles (Petkov, 2008). The technique is based on the fact that any condensed material acts as a diffraction grating when irradiated with x-rays producing a diffraction pattern that is a Fourier transform of the distribution of the *distinct* atomic pair distances in that grating (Klug and Alexander 1974). Therefore, by collecting an x-ray diffraction (XRD) pattern and Fourier transforming it the distribution of the atomic pair distances in any condensed material can be obtained. In an atomic PDF that distribution appears as a sequence of peaks starting at the shortest and continuing up to the longest distinct atomic pair distance a material shows. The areas under the PDF peaks are proportional to the number of atomic pairs occurring at the respective distances and the widths of the peaks—to the root-mean-square (rms) scatter, U_{ij}, about those distances. In particular, the full width at half maximum of a PDF peak equals $2U_{ij}\sqrt{2\ln 2}$ where i and j denote the particular atomic pair type. The atomic rms scatter amplitudes U_{ij} (see articles X-RAY POWDER DIFFRACTION and SINGLE-CRYSTAL X-RAY STRUCTURE DETERMINATION) may be dynamic (e.g., thermal) or static (e.g., due to strain) in nature reflecting correlated or uncorrelated atomic motion (Jeong et al., 1999).

An example of experimental atomic PDFs for one of the most abundant material on Earth—water, in its solid crystalline and liquid forms, is shown in Figure 1. The PDF peaks below 2 Å reflect interatomic distances within the water molecules and those at longer distances—between atoms from different water molecules. Water molecules are arranged into a long-range ordered, periodic structure with an average hexagonal symmetry in crystalline ice (Kuhs and Lehmann, 1983). The degree of structural coherence in crystalline ice is high and so the respective PDF shows a series of well-defined peaks up to very high interatomic distances. Molecules in liquid water are only short-range ordered reflecting its low degree of structural coherence (Malenkov, 2009). Accordingly, the respective PDF peaks to distances of about 1 nm only. Depending on the degree of their structural coherence, materials may show PDFs behaving like that for solid crystalline ice or that for liquid water, or like something in between. Thus by examining the profile of an experimental atomic PDF, the degree of structural coherence in a condensed material can be easily recognized. Moreover, as exemplified below, by analyzing the positions and areas of the PDF's peaks the characteristic for a particular material distribution of distinct interatomic pair distances and numbers, also known as atomic coordination sphere radii (R_i) and numbers (CN_{ij}), can be obtained over the whole length of structural coherence a material shows. For a given condensed material, the $\{R_i, CN_{ij}\}$ distribution is unique and so it can be used as its "structural fingerprint." Also, a PDF can be easily computed for any model configuration of atoms and then compared with an experimental PDF. This allows convenient testing and refining of three-dimensional structure models for materials of any degree of structural coherence. The models may be periodic or not periodic in nature allowing crystals and noncrystals to be considered on the same footing. From the model, atomic configurations important material's properties, for example, the electronic band structure and conductivity type (Petkov, 2002), may be computed and so better understood.

COMPETITIVE AND RELATED TECHNIQUES

The first Nobel prize was awarded to Wilhelm Röntgen for the discovery of x-rays back in 1901. The Nobel prize in 1914 went to Max von Laue for the discovery of x-rays diffraction in crystals. Since then x-ray diffraction has been a major scientific tool for the determination of the structure of single crystals. The techniques benefits from the fact that several independent diffraction patterns can be collected for different orientations of the single crystal specimen with respect to the x-ray beam (Giacovazzo, 1998). The recorded several tens to many hundreds or even thousands sharp diffraction spots, also known as Bragg peaks, provide a firm basis for the determination of the atomic-scale structure of single crystals from simple solids to proteins (see also SINGLE-CRYSTAL X-RAY STRUCTURE DETERMINATION). The atomic PDF resembles the so-called Patterson function that is widely used in traditional crystallography (Giacovazzo, 1998). However, while the Patterson function peaks at interatomic distances within the unit cell of a crystal, the atomic PDF peaks (see Fig. 1) at all distinct interatomic distances occurring in a material. Interatomic distances of different spatial orientations but same magnitude will come as a single PDF peak since the atomic PDF is one dimensional, spherically, that is, all atomic-scale structure orientations averaged representation of the respective diffraction grating/material (see Fig. 2). For this reason, atomic PDFs analysis has little advantage to offer in single crystal structure studies. Its advantages are much more obvious in studying the atomic-scale structure of materials that are not perfect single crystals in nature.

Typical polycrystalline materials consist of a large number of randomly oriented crystallites. As a result, polycrystalline materials exhibit one-dimensional diffraction patterns where all atomic-scale structure

Characterization of Materials, edited by Elton N. Kaufmann.

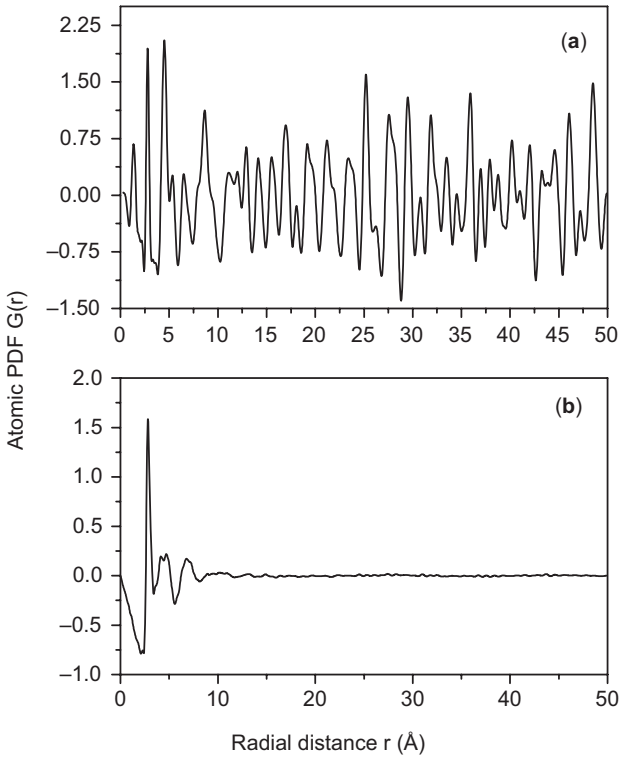

Figure 1. Experimental atomic PDFs for solid crystalline (**a**) and liquid water (**b**).

orientations are randomly, that is, spherically averaged (see article X-ray Powder Diffraction). Although the structure orientations are averaged out in x-ray powder diffraction patterns they still show several tens up to a few hundred sharp Bragg peaks allowing a successful crystal structure refinement and even determination to be carried out in an almost routine way (David et al., 2002; Samy et al., 2010). Depending on their degree of structural coherence materials will show powder diffraction patterns with only sharp Bragg peaks (e.g., crystalline ice) or only broad, diffuse-type diffraction features (e.g., water), or both. Powder diffraction analysis mostly concentrates on the sharp Bragg peaks and considers them in terms of structure models based on infinite periodic lattices (Hahn, 2002). On the other hand, atomic PDFs analysis uses both the Bragg peaks and the diffuse-type scattering components in the diffraction pattern. In this way both the existing atomic order, manifested in the Bragg-like peaks, and all structural "imperfections" (e.g., strain, defects, very small/nanosize particle's dimension) that are responsible for its limited extent, manifested in the diffuse component of the diffraction pattern, are reflected in the experimental PDFs. This renders the atomic PDFs analysis much better suited to study materials where the periodicity of the atomic arrangement is partially broken due to local structural distortions (Petkov, 1999) or the atomic arrangement is not periodic at all (Roux et al., 2011). In this respect, atomic PDFs analysis goes beyond traditional powder x-ray diffraction analysis that yields only the periodic features of the atomic-scale structure.

Spectroscopy techniques such as expended x-ray absorption fine structure (EXAFS) and nuclear magnetic resonance (NMR) are also frequently used to study the local atomic arrangement in materials, including determining of atom–atom separations and coordination numbers (Czichos et al., 2006; see articles NMR Spectroscopy in the Solid State and XAFS Spectroscopy). These techniques have a better atomic species sensitivity (less than 1 at%) than x-ray diffraction-based atomic PDFs analysis (down to few atomic percent). Spectroscopy techniques, however, yield structural information related not to all present but only to the particular atomic species probed. Besides, this information is limited to interatomic distances up to 5–6 Å only.

Imaging techniques such as high-resolution transmission electron microscopy (TEM) can provide information about material's structure with atomic resolution (Czichos et al., 2006; see articles Scanning Electron Microscopy and Transmission Electron Microscopy). However, as any other image, TEM images are just a projection down an axis and so are not easy to be interpreted in terms of a unique three-dimensional atomic arrangement. The situation may change for better with the recent advances in TEM tomography (Midgley and Dunin-Borkowski, 2009). Nevertheless, data from present day EXAFS and TEM experiments are very useful, in particular in providing independent constraints for structure modeling guided by atomic PDFs (Roux et al., 2011).

PRINCIPLES OF THE METHOD

Atoms in condensed matter interact via chemical bonds that impose preferred atom–atom separations and coordination numbers that do not change a lot even when a material appears in phase states of very different structural coherence. For example, both quartz crystals (SiO_2) and silica glass (SiO_2) are made of rigid $Si–O_4$ tetrahedral units that share all of their corners. The difference is that in quartz crystals, the tetrahedra are assembled into a periodic network of hexagonal symmetry (Page and Donnay, 1976), whereas in the glass that network is completely random (Zachariasen, 1932). The situation with crystalline ice and water is similar (Malenkov, 2009) regardless of the fact that the hydrogen–oxygen bonds in it are much weaker than the Si-O covalent bonds in silicates. Given the presence of well-defined chemical bonds and the imposed by them distinct atom–atom separations and coordination numbers, a quantity called atomic pair distribution function can be defined for any condensed material. In particular, the frequently used reduced atomic PDF, $G(r)$, gives the number of atoms in a spherical shell of unit thickness at a distance r from a reference atom as follows:

$$G(r) = 4\pi r[\rho(r) - \rho_o] \quad (1)$$

where $\rho(r)$ and ρ_o are the local and average atomic number densities, respectively. As illustrated in Figure 2, the atomic PDF is a one-dimensional function that oscillates

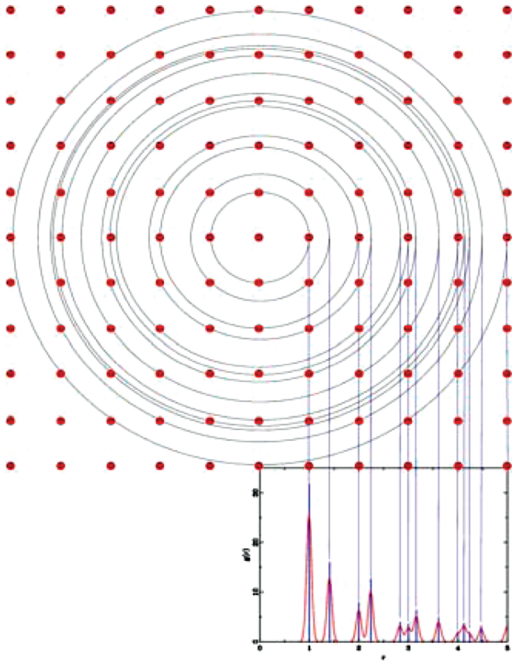

Figure 2. Spherically averaged distribution of interatomic distances and numbers in a hypothetical square lattice of atoms (points). The distribution peaks at distances separating pairs of atoms; peak areas are proportional to the number of atoms at those distances.

around zero and shows positive peaks at distances separating distinct pairs of atoms, that is, where the local atomic density exceeds the average one. As demonstrated in Figure 1, the oscillations are very pronounced and characteristic to the particular phase state of the studied material. Since the wavelength of x-rays is comparable to the distances between atoms in condensed matter, x-rays can scatter constructively from the grating of uniformly separated and coordinated atoms in a condensed material. Moreover, the resulted diffraction pattern reflects the spatial characteristics of that grating (Giacovazzo, 1998; Klug and Alexander 1974). Indeed, the PDF $G(r)$ is the exact Fourier transform of the atomic-scale structure sensitive part of the scattered x-ray intensities, also known as structure function, S(Q), that is,

$$G(r) = (2/\pi) \int_{Q=Q_{\min}}^{Q_{\max}} Q[S(Q)-1]\sin(Qr)dQ \qquad (2)$$

where Q is the magnitude of the wave vector ($Q = 4\pi\sin\theta/\lambda$), 2θ is the angle between the incoming and outgoing x-rays and λ is the wavelength of the x-rays used (Wagner, 1969). Note the structure function, $S(Q)$, is related to only the coherent/elastic part of the scattered x-ray intensities, $I^{\text{coh.}}(Q)$, as follows:

$$S(Q) = 1 + \left[I^{\text{coh.}}(Q) - \sum c_i |f_i(Q)|^2\right] \Big/ \left|\sum c_i f_i(Q)\right|^2, \quad (3)$$

where c_i and $f_i(Q)$ are the atomic concentration and x-ray scattering factor, respectively, for the atomic species of type i. Note, other definitions of $S(Q)$ and the atomic PDF are also known but less frequently used (Keen, 2001). Also, the integral in Equation 2 is taken from $Q_{\min}$ to $Q_{\max}$ where the former is the lowest (typically of the order of 0.3–0.5 Å^{-1}) and the latter the highest wave vectors, respectively, reached in the diffraction experiment. In other words, in this common derivation of $G(r)$ the small-angle scattering intensities that appear at wave vectors approaching zero are not included. If those were included a modified atomic distribution function, $G'(r) = 4\pi r[\rho(r) - \gamma_o(r)\rho_o]$ would be obtained, where $\gamma_o(r)$ is function reflecting large-scale density fluctuations in the material studied, including the shape of its constituent crystallites/particles (Farrow and Billinge, 2009). No examples of atomic PDF studies that incorporate small-angle scattering intensities are known yet, though this may change in future. In this review article, we stick to the common derivation (given in Equations 1, 2 and 3) and usage of atomic PDFs that do not include small-angle scattering information. Within this common derivation, the integral in Equation 2 can be represented in a discrete form to take into account the discrete nature of XRD experiment, that is,

$$G(r_k) = (2/\pi) \sum_{i=1}^{N} Q_i[S(Q_i)-1]\sin(Q_i r_k)\Delta Q \qquad (4)$$

where N is the number of actual experimental data points, Q_i, collected in equidistant ΔQ steps as usually done in XRD studies. Here r_k is a real-space distance at which $G(r)$ has been chosen to be evaluated. For practical purposes $G(r)$ is also evaluated at a number of equidistant real space distances $r_k = k\Delta r$ points, where k is an integer number. Typically Δr is of the order of 0.01 to 0.05 Å. However, following the Nyquist-Shannon sampling theorem the step Δr is best to be set close to $\pi/Q_{\max}$ (Thijsse, 1984; Farrow et al., 2011).

Therefore, to obtain an experimental atomic PDF an XRD data set should be collected, only the coherent part, $I^{\text{coh.}}(Q)$, of the collected intensities extracted, reduced to a structure factor S(Q) (Equation 3) and then Fourier transformed (Equations 2 and 4). For a material comprising n atomic species a single diffraction experiment would yield a total atomic distribution function, $G(r)$, which is a weighted sum of $n(n+1)/2$ partial PDFs, $G(r_{ij})$, that is,

$$G(r) = \sum_{i,j} w_{ij} G_{ij}(r), \qquad (5)$$

where w_{ij} are weighting factors (Wagner, 1969) depending on the concentration and scattering power of the atomic species as follows:

$$w_{ij} = c_i c_j f_i(Q) f_j(Q) \Big/ \left|\sum c_i f_i(Q)\right|^2. \qquad (6)$$

For practical purposes w_{ij}'s are often evaluated for $Q = 0$.

A total PDF for a multielement material, however, will comprise quite a few partial atomic correlations which may render its interpretation ambiguous.

Element specificity may be added by employing the so-called resonant XRD, which involves measuring two diffraction data sets close to but below the absorption edge of an atomic species, taking the difference between these two data sets, and Fourier transforming it into a quantity called a differential atomic PDF. Similarly to EXAFS spectroscopy, the differential atomic PDF will reflect only correlations relative to the element whose absorption edge is probed. However, unlike EXAFS, it will show these correlations to the longest interatomic distances to which they extend (Petkov and Shastri, 2010). As demonstrated recently, differential atomic PDFs can be very useful in revealing very fine structural features of complex materials (Petkov et al., 2010a).

PRACTICAL ASPECTS OF THE METHOD

To ensure good quality results XRD experiments aimed at atomic PDFs analysis should be conducted paying special attention to the following details:

Source of X-ray Radiation: XRD data up to high wave vectors should be collected so that the respective atomic PDF is of good enough real-space resolution to reveal all important structural features of the material studied. High-wave vectors can be reached by employing x-rays of a shorter wavelength, that is, of higher energy. For example, by using synchrotron radiation x-rays of energy 60 keV (Petkov et al., 1999) structure functions for (In–Ga)As semiconductors extending to $Q_{max} = 45$ Å^{-1} were possible to be obtained (see Fig. 3). The respective atomic PDFs have an excellent real-space resolution, $\delta r = 2\pi/Q_{max} = 0.14$ Å, allowing to reveal the presence of distinct Ga–As (2.44 Å) and In–As (2.61 Å) bonds in this semiconductor alloy (see Fig. 4). If x-rays of energy 8 keV (Cu K_α radiation) or 22 keV (Ag K_α) radiation were used XRD data would have been possible to be collected to Q_{max} values of approximately only 8 Å^{-1} and 20 Å^{-1}, respectively (see the broken lines in Fig. 3). Using XRD data with $Q_{max} = 20$ Å^{-1} in the Fourier transformation of Equation 2 and 4 would not have allowed to resolve the distinct Ga-As and In-As bonds but yet allowed to reveal well the characteristic sequence of coordination spheres in (In–Ga)As semiconductor alloys (see Fig. 5). Using XRD data with $Q_{max} = 8$ Å^{-1} would have produced a very low-resolution PDF where the individual peaks are merged (see the 5–8 Å region in Fig. 5) beyond recognition. Such low real-space resolution PDF data may be very misleading, leading to erroneous interpretation. The example emphasizes the importance of collecting and using XRD data up to as high wave vectors as possible in atomic PDF studies. This can be achieved on in house equipment using sealed x-ray tubes with a Mo or better Ag and definitely not Cu anode, or by employing higher energy synchrotron radiation sources.

XRD Data Statistics and Collection Time: Regardless of the source of high-energy x-rays used the diffraction data should be collected with a very good statistical accuracy, usually 2–3 orders of magnitude better than

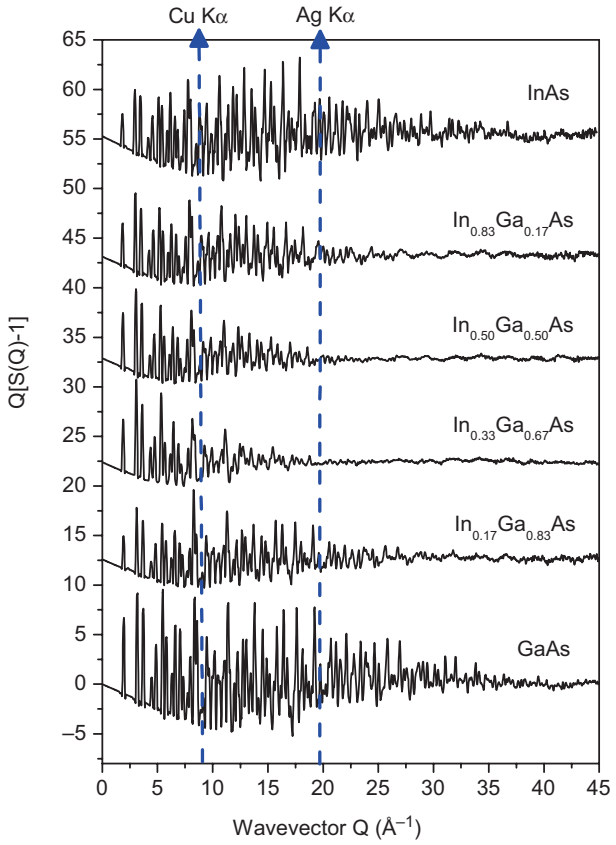

Figure 3. Experimental structure factors for (In–Ga)As semiconductor alloys obtained with synchrotron x-rays of energy 60 keV ($\lambda = 0.205$ Å). Broken lines show the maximum wave vector Q that could have been reached if CuK_α ($\lambda = 1.54$ Å) or AgK_α ($\lambda = 0.509$ Å) radiation were used instead.

that required for traditional powder XRD (e.g., Rietveld analysis) studies. An example illustrating the importance of collecting XRD of good statistical accuracy is given in Figure 6. An XRD pattern for 5 nm CdTe quantum dots (QDs) collected with 10^4 counts per Q_i data point yields a structure function that is of good statistical accuracy at low-Q values only. Due to the presence of a multiplicative Q factor in the kernel of the Fourier transformation (see Equation 2) the data noise, that is, hardly visible at low-Q values, appears greatly amplified at higher wave vectors. Following the Fourier transformation this data noise leads to pronounced high-frequency ripples throughout the respective atomic PDF. The ripples distort its profile and even may be falsely taken for "real" interatomic distances. An XRD pattern collected with 10^6 counts per Q_i data point yields an almost noise free structure factor and an atomic PDF revealing the atomic-scale structure of CdTe QDS in very accurate detail (Pradhan et al., 2007). To achieve good statistical accuracy obviously longer than usual XRD data collection time is necessary to be used. Data collection time estimates relevant to atomic PDF studies are discussed in (Toby and Egami, 1992; Peterson et al. 2003; Mullen and Levin, 2011). Also, the step ΔQ (or the equivalent to it step in the Bragg angles) with which the XRD data are

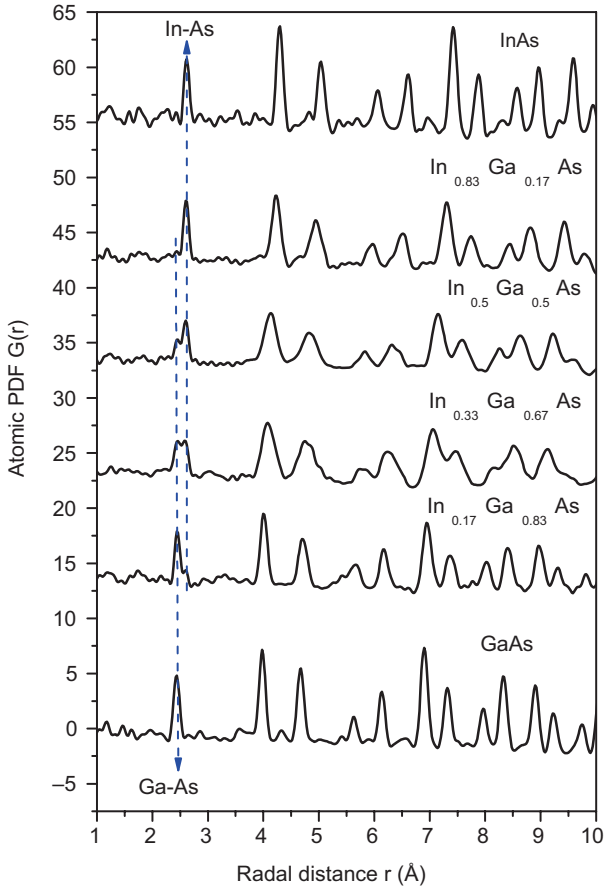

Figure 4. Experimental PDFs for (In–Ga)As semiconductors obtained by Fourier transforming the structure factors of Figure 3. Broken lines with arrows mark the shortest Ga–As (2.44 Å) and In–As (2.61 Å) bond lengths in the alloy samples.

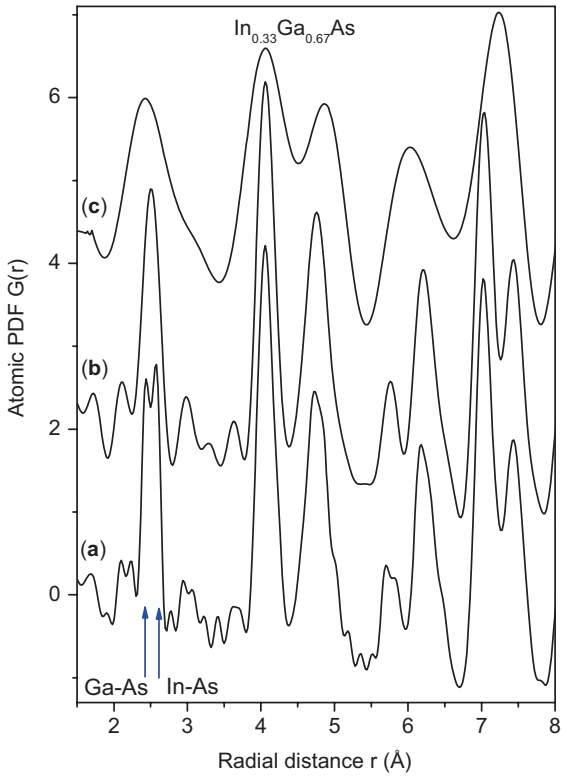

Figure 5. Experimental PDFs for $In_{0.33}Ga_{0.67}As$ alloy obtained by Fourier transforming the respective structure factor of Figure 3 with Q_{max} set to 45 Å^{-1} (**a**), 20 Å^{-1} (**b**), and 8 Å^{-1} (**c**). Arrow marks the shortest Ga–As (2.44 Å) and In–As (2.61 Å) bond lengths in this material. Those are clearly resolved only when XRD data collected up to 45 Å^{-1} are included in the Fourier transformation.

collected should be small enough (e.g., ensuring at least 5–7 Q_i data points under a Bragg-like peak) so that no fine diffraction features are missed. In total, all this may result in many tens of hours of data collection time per sample if a sealed x-ray tube source and a single point (e.g., scintillation) detector are employed. Synchrotron x-rays and large area detectors may reduce the data collection time to seconds (Chupas et al., 2003; Lee et al., 2008a).

Experimental Setup (Q-space) Resolution: In general, structure studies on materials of limited structural coherence do not require experimental setups with very high reciprocal (Q)-space resolution because of the inherently diffuse nature of the XRD patterns such materials show. However, care should be taken that the reciprocal space resolution of the experimental set up, including the detector, is not too low either. As an example, atomic PDFs for $BaZr_{0.1}Ti_{0.9}O_3$ ceramics obtained from XRD data sets collected with two different types of detectors, an image plate (IP) detector, and a detector set of 12 single crystals (Lee et al., 2008b) are shown in Figure 7. The quite low Q-space resolution of the XRD data collected with an area IP detector, that is, the quite large detector introduced broadening of the XRD peaks, leads to a very fast, unphysical decay (Qiu, 2004a) in the respective atomic PDF. As a result, it appears completely flat for distances above 50–60 Å that are much shorter than the actual length of structural coherence in these ceramics. By contrast, the much higher Q-space resolution of the XRD data collected with the detector set of 12 single crystals results in an atomic PDF showing physical oscillations, that is, the presence of distinct atomic coordination spheres, to very high interatomic distances allowing studying of long-range atomic ordering effects. Therefore, to avoid unwanted loss of information in the higher region of atomic PDFs, the Q-space resolution of the experimental set up, in particular that of the detector, should be adjusted accordingly.

Finite Particle's Size Effect on Atomic PDFs: Atomic PDFs analysis is very well suited to study the atomic arrangement in nanosized particles (Gilbert et al., 2004; Petkov, 2008). The finite size and highly anisotropic shape of nanosized, in particular 1–10 nm in size, particles may affect the shape and intensity of the peaks in experimental atomic PDFs substantially (Petkov et al., 2009). The effect of particle's finite size on the atomic PDFs is somewhat similar to that of the low-Q space resolution discussed above so care should be taken that those are not confused with each other. The finite particle's size effect can be taken into account by using appropriate particle's shape functions (Kodama

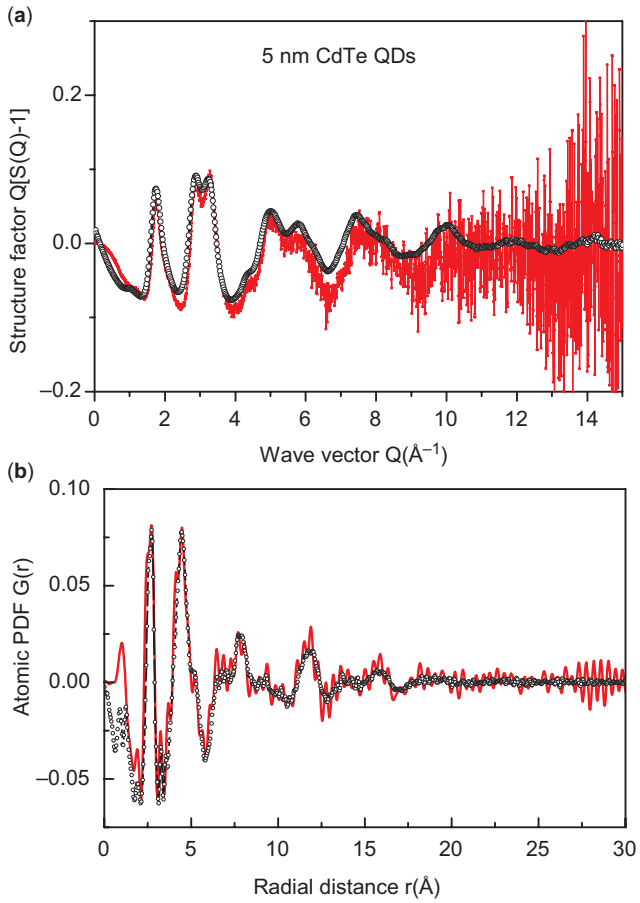

Figure 6. Experimental structure factors for 5 nm CdTe quantum dots (QD)s collected with 10^4 (full line in gray) and 10^6 (symbols) counts per data point (**a**). The respective atomic PDFs are shown in (**b**). That obtained from the data set of lower statistical accuracy suffers pronounced high-frequency, unphysical ripples.

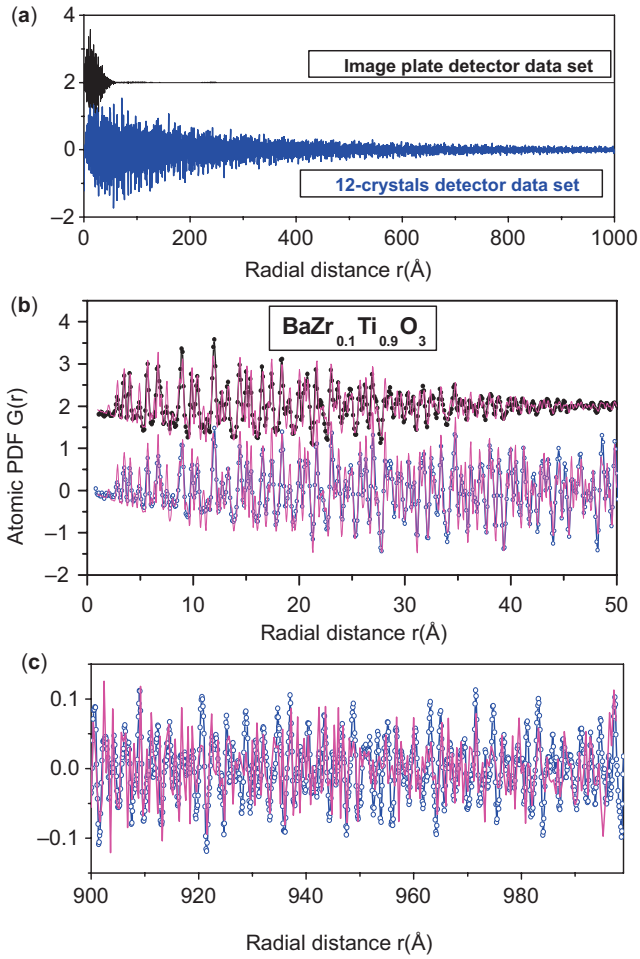

Figure 7. (**a**) Experimental atomic PDFs for BZT ceramics obtained with an image plate detector (line in black) and a detector set of 12 single crystals (line in dark gray). The low Q-resolution image plate detector yields an atomic PDF that decays to zero at distances of 50–60 Å that are much shorter than the average domain size in the ceramics material studied. The higher Q-resolution detector set of 12 crystals yields an atomic PDF that shows physical oscillations up to distances of 1000 Å, and more, that are comparable to the average domain size in this material. (**b**, **c**) Fragments of the experimental PDF data as fit with a model featuring the well-known perovskite structure of BZT (line in light gray). Experimental and model PDF's peaks match well to very high interatomic distances confirming the physical origin of the PDF's oscillations.

et al. 2006; Farrow et al., 2007) or by building finite size, real particle's shape structure models (Korsunsky et al., 2007; Petkov et al., 2010b).

Background Scattering Treatment: Air, sample holder etc. background-type scattering should be kept to a minimum since atomic PDFs are related to only the coherent/elastic part, $I^{coh.}(Q)$, of the x-ray intensities scattered from the sample alone (see Equation 3). As practice has repeatedly shown it is always easier to correct for a weak background signal than for a strong one. Therefore, as high as possible sample to background scattering ratio is recommended, especially at high wave vectors where that ratio should at least be of the order of 4–5 to 1. Once reduced to a minimum, the background scattering should be measured with the same statistical accuracy as the sample scattering and so used in the process of reducing the experimental XRD data into an atomic PDF.

Sample Related "Unwanted" Scattering: X-rays are both scattered from and absorbed inside materials via various processes (Klug and Alexander, 1974). The absorption of high-energy x-rays is relatively low and usually does not pose much of a problem in atomic PDFs studies. The same is true for multiple scattering of high-energy x-rays. As illustrated in Figure 8, inelastic (Compton) scattering, however, may be very strong and even exceed the elastic scattering, especially at high wave vectors (Petkov, 2002). Inelastic, that is, scattered with modified energy x-ray photons should be eliminated from the experimental XRD pattern since only its coherent/elastic part is related to the atomic PDF (see Equation 3). The elimination is best to be done during data collection by using x-ray energy sensitive detectors (Ruland, 1964; Petkov, 1999, 2000). Alternatively, it can

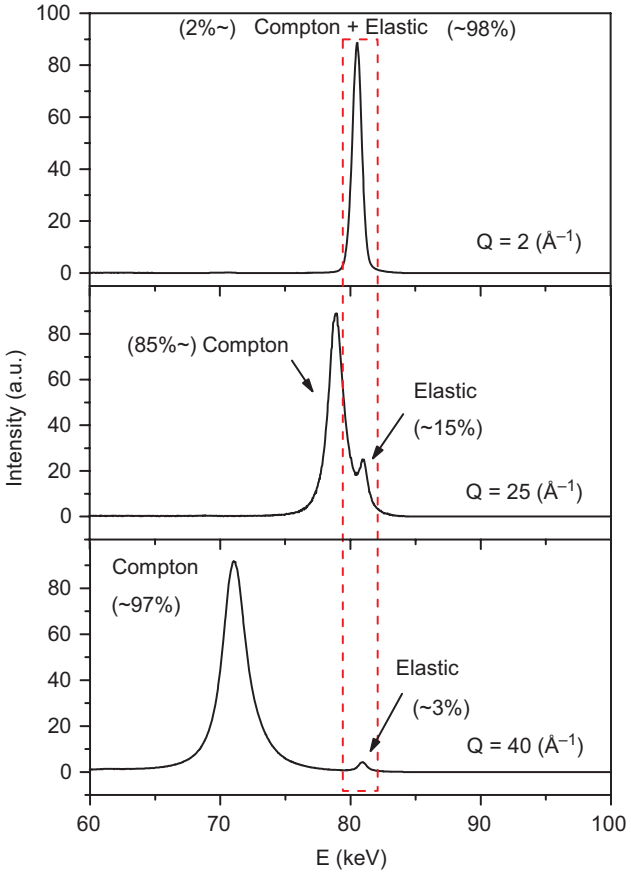

Figure 8. X-ray scattered intensities versus x-ray energy spectra from $Ca_{0.25}Al_{0.5}Si_{0.5}O_2$ glass collected at three different wave vectors, Q. Data were taken with x-rays of energy 80.6 keV (Petkov et al., 1999). Note the dramatic decrease of the coherent/elastic scattering (marked with broken line in red) with the increase of Q.

be done analytically during the reduction of the experimental XRD data into an atomic PDF. The analytical elimination of Compton scattering is, however, inevitably based on some theoretical approximations (Hajdu and Palinkas, 1972) which may lead to difficulties (Qiu, 2004a) in obtaining good quality atomic PDF data.

METHOD AUTOMATION

Atomic PDFs analysis is fully automated in all of its aspects, including XRD data collection, XRD data reduction into atomic PDFs, the interpretation of experimental PDFs in terms interatomic distances and numbers, and atomic PDFs guided structure modeling rendering the technique a rather convenient and useful scientific tool.

XRD data of quality good enough for a successful atomic PDFs study can be collected on in-house equipment for powder XRD. However, instead of the standard Cu K_α radiation source, x-ray tubes with a Mo or Ag anode or rotating (Mo or Ag) anode sources should be employed so that the XRD data are collected to at least 15–20 Å^{-1}. Also, extra care should be exercised to reduce the inherently high background scattering inside the enclosures of the standard powder XRD instruments. XRD data of quality good enough for a successful PDF study are much easily collected at synchrotron radiation sources because of the much higher intensity and energy of the x-rays produced by them allowing Q_{max} values of 30–45 Å^{-1} to be achieved. Several beam lines at numerous synchrotron radiation facilities are available all over the world, including instruments entirely dedicated to atomic PDFs studies (Chupas et al., 2003; Lee et al. 2008a; Kohara et al., 2001).

Software for correcting experimental XRD patterns for background and other "unwanted" scattering as well as for x-ray absorption, polarization, detector dead time and x-ray energy resolution, normalizing the corrected intensities into absolute units, reducing them into structure functions $S(Q)$, and finally performing a Fourier transformation to obtain an atomic PDF is readily available (Petkov, 1989; Qiu, 2004b; Soper and Barney, 2011).

Positions and areas of peaks in experimental atomic PDFs can be extracted with the help of any software package used for visualization, manipulation, and plotting of scientific data.

Relatively small-size (up to few hundred atoms) structure models based on periodic (Bravais) lattices can be conveniently built, tested, and refined against experimental atomic PDFs with the help of the program PDFgui (Farrow et al., 2007).

Large-scale (many thousands of atoms) structure models featuring pronounced local disorder can be built, tested, and refined against experimental atomic PDFs with the help of the program DISCUS (Neder and Proffen, 2008).

Completely, nonperiodic model atomic configurations featuring glasses and liquids can be tested and refined against experimental PDF data employing reverse Monte Carlo (Gereben et al., 2007) or molecular dynamics (Lindahl et al., 2001) type procedures.

Once constructed, structure models for materials of limited structural coherence can be analyzed in terms of bond length, bond angle, and partial coordination number distributions, topological connectivity, local symmetry, and other structural characteristics with the help of the program ISAACS (Roux and Petkov, 2010).

ATOMIC PDF DATA ANALYSIS AND INTERPRETATION

An experimental atomic PDF carries a wealth of atomic-scale structure information. Some pieces of it are immediately evident in the PDF data, others need applying of extra analytical procedures to be extracted and fully exploited.

An important material's characteristic that is evident in the experimental atomic PDFs is the material's phase type (e.g., see Fig. 1). Here a phase means a part of a material that has a well-defined chemical composition and atomic-scale structure, is physically and chemically homogeneous within itself and so is surrounded by a boundary that makes it mechanically separable from the rest of the material and/or the material's environment. Bragg XRD is a major tool for qualitative phase

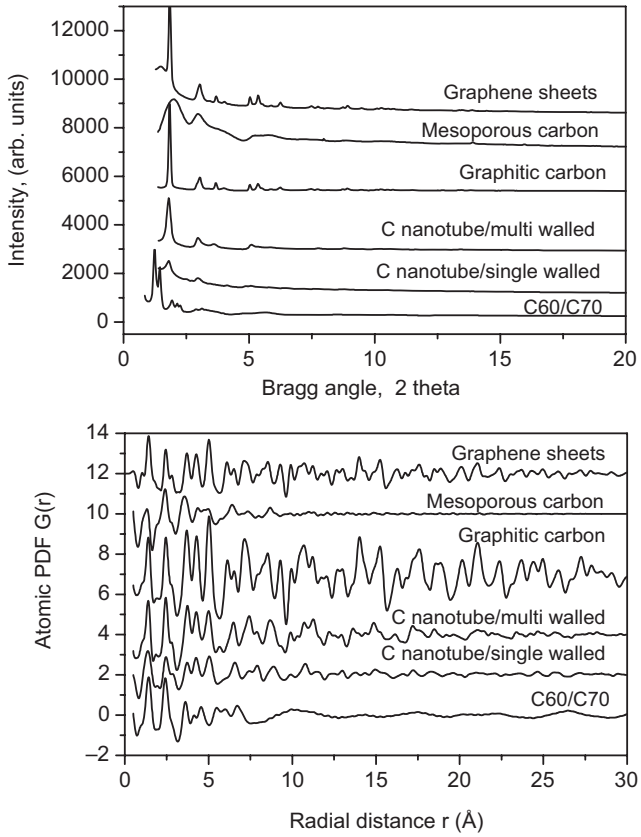

Figure 9. Experimental XRD patterns (up) and the respective atomic PDFs (down) for a series of graphitic carbons.

identification of crystalline materials. XRD patterns for materials of limited structural coherence, however, are usually quite diffuse in nature and so are difficult to be used for unambiguous phase identification. Atomic PDFs can be employed instead. As an example, experimental XRD patterns and atomic PDFs for a series of nanosized graphitic materials are shown in Figure 9. The XRD patterns show only a few Bragg-like features, whereas the respective atomic PDFs show numerous peaks coming from the sequence of well-defined atomic coordination spheres in these graphitic materials. Since carbon atoms in the different graphitic materials are arranged differently (e.g., forming stacks of flat sheets in graphitic carbons, folded sheets in the nanotubes, and spheres in the C_{60} fullerenes) the respective experimental PDFs are substantially different and so can be used to identify each of the respective graphitic phases. Reference databases of atomic PDFs can be generated for important classes of materials of limited structural coherence (e.g., for silicate glasses, industrial amorphous polymers, and pharmaceuticals) and used for their qualitative phase identification in a manner similar to that implemented in the so-called Powder Diffraction File with XRD patterns of crystals (Smith and Jenkins, 1996). Examples of successful application of atomic PDFs analysis for determining the relative fraction of phases in a mixture, that is, for quantitative phase analysis are known as well (Gateshki et al., 2007).

Another important material's characteristic is the length of structural coherence, also known as the mean size of coherent x-ray scattering domains (Klug and Alexander, 1974). Atoms from different domains are not well lined up and so do not make consecutive sequences of well defined atomic coordination spheres. Accordingly, the peaks in the atomic PDFs suffer extra loss of sharpness for distances longer than the "domain size" rendering the atomic PDF featureless beyond those distances. The fact is well demonstrated in Figure 10 showing experimental atomic PDFs for crystalline Au and nanosized Au particles (Petkov et al., 2005a). The smaller the particles, the shorter the real space distance at which the respective atomic PDF decays to zero. It goes from about 50 Å for 30 nm down to 10 Å for 1.7 nm particles. Note, the length of structural coherence in the particles is shorter than their actual size since the particles (see Fig. 11A for a structure model of 3 nm particles) exhibit extended structural defects, resembling wedge disclinations, dividing their inner part into domains that are misoriented with respect to each other. Care should be taken that the behavior of the longer part of the experimental PDFs is not dominated by low Q-space resolution effects (see Fig. 7) when the length of structural coherence is the quantity of interest. Correction procedures for moderate Q-space resolution effects are discussed in (Gateshki et al., 2005).

The commonly used atomic PDF $G(r)$ (see Equations 1 and 2) slopes as $4\pi\rho_o^* r$ for small r values, in particular in the region from $r=0$ to about $r=1$ Å where no real interatomic distances exist. Therefore, estimates for the atomic number density ρ_o (i.e., density measured in atoms/Å^3) of the material studied can be obtained from the initial slope of experimental $G(r)$ data as illustrated in Figure 10. Note since XRD experimental errors tend to add up close to the origin of the Fourier transformation (Peterson et al., 2003; Qiu, 2004a), that is, close to $r=0$ Å, the ρ_o estimate should be done with due care.

Atomic coordination numbers, CN_{ij}, are another important structural parameter. They can be derived from the area of the respective PDFs peaks. As defined the atomic PDF $G(r)$ oscillates about zero (see Equation 1 and Fig. 1) making it inconvenient for integrating its peaks for the purpose of obtaining an estimate for the peak's areas. Another atomic PDF defined as:

$$RDF = 4\pi r^2 \rho(r) = 4\pi r^2 \rho o + r^* G(r) \qquad (7)$$

where r is the radial distance, and $\rho(r)$ and ρ_o the local and average atomic number densities, respectively, is better to be used in this case. From the integrated RDF peak areas, the number of atomic neighbors of type j around atomic species of type i, that is, CN_{ij}, can be obtained as follows:

$$CN_{ij} = c_j^*(\text{respective RDF Peak Area})/w_{ij} \qquad (8)$$

where the atomic concentrations c_j and the weighting factors w_{ij} (see Equation 6) should strictly obey the sum

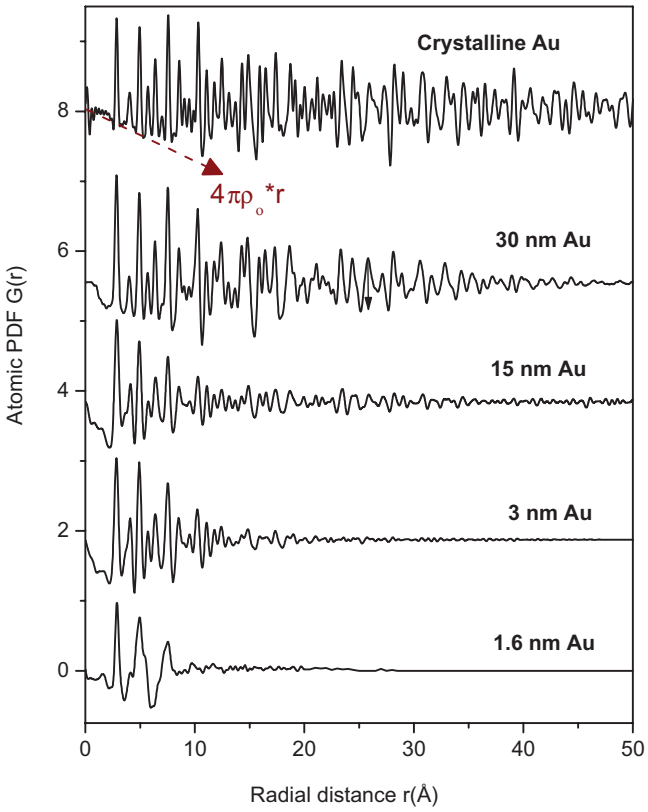

Figure 10. Experimental atomic PDFs for crystalline (μm-sized) and nanosized Au particles (Petkov et al., 2005a). Arrow marks the low-r PDF region that slopes as $4\pi\rho_o{}^* r$.

rules $\sum c_j = 1$ and $\sum w_{ij} = 1$. Note the area of a PDF/RDF peak is not simply proportional (via the c_j term in Equation 8) to the number of respective atomic pairs CN_{ij} but depends on the atomic pair's relative scattering power (via the w_{ij} term in Equation 8) as well. Therefore, for accurate estimates of CN_{ij} to be obtained, Equation 8 should be strictly applied. The areas of individual RDF peaks can be obtained by a direct integration when those peaks are well resolved. When the RDF peaks are partially overlapped, which is often the case, the individual peak areas can still be evaluated very precisely by fitting each peak with a Gaussian function as demonstrated in Figure 12. In this example, the first coordination numbers of Si, Al, and Ca atoms in $Ca_{x/2}Al_xSi_{1-x}O_2$ glasses are obtained allowing to draw important conclusions about the type of coordination units and their connectivity in the glass network (Petkov et al., 2000).

The ultimate goal of structure studies is the determination of the positions of the atoms constituting the material under study. In case of crystalline-like materials, PDFs analysis can yield the positions of atoms within the unit cell of a periodic lattice by using available software (Farrow et al., 2007, Neder and Proffen, 2008). At first, a structure model featuring a unit cell of a periodic lattice is designed using theoretical predictions or available crystal structure data for materials of similar chemistry. The sequence of coordination radii and numbers (r_i, CN_{ij}) for that model is computed and then convoluted with gaussians to take into account the thermal and eventually static atomic rms displacements in the material under study. Thus computed model PDF is compared to the experimental one and the difference between the experimental and model PDF data minimized by adjusting the atomic positions and rms displacements in the initial model. Example of a determination of the structure of a crystalline-like material via atomic PDF analysis is shown in Figure 11c. Nonperiodic type structure models that are more appropriate for liquids and glasses can also be tested and refined against atomic PDFs using available software (Gereben et al., 2007; Lindahl et al., 2001). In this case, the model is a large-scale atomic configuration of many thousand atoms that is a statistically representative fragment of the material under study. An example is shown in Figure 11b. Finite size models, that is, models not subject to periodic boundary conditions, that are very appropriate for nanosized metallic particles (see Fig. 11a), semiconductor quantum dots (Pradhan

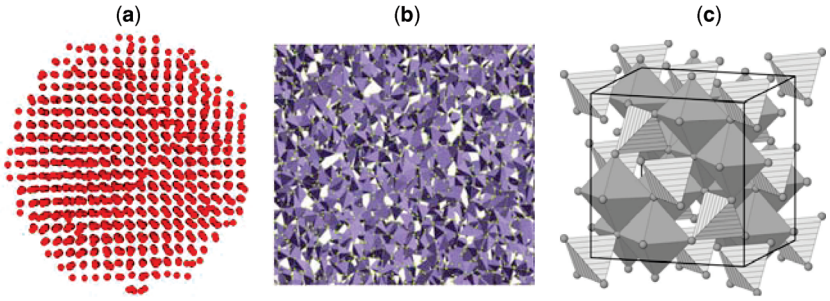

Figure 11. Structure models of 3 nm Au particles (**a**), $GeSe_2$ glass (**b**), and Mg ferrite (**c**) derived from fits to the respective experimental atomic PDFs. The model for Au particles features atoms (red circles) arranged in an face-centered cubic type structure (Petkov et al., 2005a). The model for $GeSe_2$ glass feature a random network of corner and edge-sharing Ge-Se_4 tetrahedra (Petkov and Messurier, 2010). The model (Gateshki et al., 2005) for Mg ferrite features a periodic cubic lattice of Fe-O_6 octahedral (gray) and Fe-O_4 tetrahedral units (shaded).

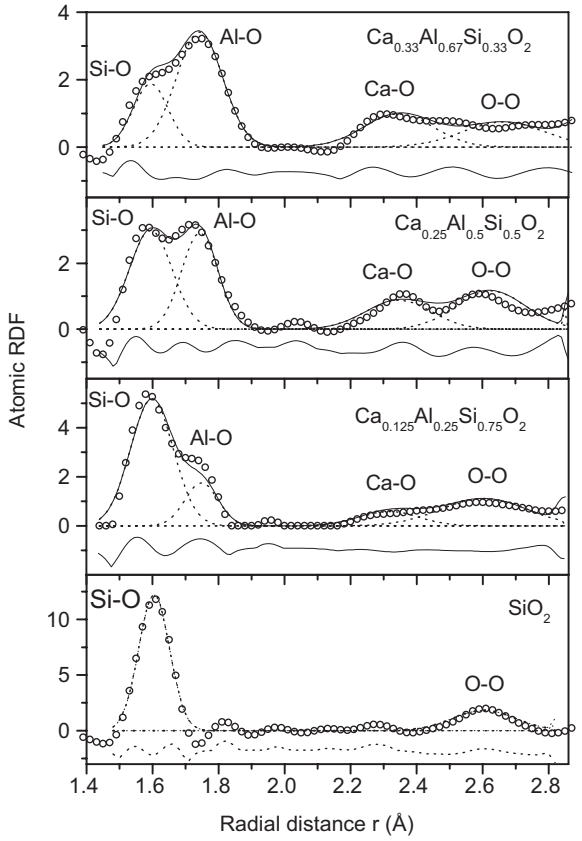

Figure 12. Gaussian fit to the first peaks in the RDFs for $Ca_{x/2}Al_xSi_{1-x}O_2$ ($x = 0$, 0.25, 0.5, 0.67) glasses. Experimental data: symbols; fitted data: full line; individual Gaussians: broken line; residual difference: full line (bottom). Peaks are labeled with the corresponding atomic pairs.

et al., 2007), or large organic molecules (Petkov et al., 2005b) can also be tested and refined against atomic PDFs. Successful attempts of using atomic PDFs for *ab initio* structure determination are also known (Juhas et al., 2006). In the atomic PDF-based structure determination process, plausible constraints based on a priori knowledge about material's chemistry, density, local coordination (e.g., from complimentary NMR or EXAFS experiments), and others are often needed to be employed to discriminate between competing solutions. Note, atomic PDFs are one-dimensional, spherically averaged representation of the atomic arrangement so the uniqueness of the three-dimensional structure solution found by atomic PDFs analysis is not always guaranteed.

SAMPLE PREPARATION

Atomic PDFs analysis can be done on samples of any size, shape, and phase state so long those can be mounted on a typical in-house or synchrotron XRD instrument. No special sample preparation is necessary though optimizing the sample size and shape with respect to maximizing the scattered intensities and reducing sample-related unwanted scattering is highly recommended, anytime it is possible. Also, a careful choice of the XRD data collection geometry, that is, reflection versus transmission versus capillary, should be made according the particular sample's phase state (Klug and Alexander, 1974; Thijsse, 1984).

SPECIMEN MODIFICATION

X-ray diffraction is a nondestructive technique. Samples measured remain completely unaltered which is a great advantage comparing with other material's structure characterization techniques such as electron microscopy and diffraction for example. Rarely organic materials can become damaged by the high flux of synchrotron radiation x-rays. Therefore, such samples should not be overexposed but only measured as long as necessary to obtain good statistical accuracy.

PROBLEMS

Typical problems include distortions of the PDFs peak shape (e.g., see Fig. 5), appearance of false PDF peaks (e.g., see Fig. 6) and/or shifts in PDFs peaks positions due to misalignment of the XRD instrument or errors in the x-ray wavelength calibration. Various sources of errors and their particular effect on atomic PDFs are discussed in (Peterson et al., 2003; Qiu et al., 2004b; Petkov and Danev, 1998). To minimize errors in atomic PDFs: (i) the XRD instrument should be carefully aligned, (ii) x-ray wavelength well calibrated, (iii) background and sample-related unwanted scattering minimized by a careful optimization of the experimental setup, (iv) XRD data taken to high wave vectors, (v) in appropriate ΔQ steps, and (vi) each with a very good statistical accuracy. Estimates for the latter are given in (Toby and Egami, 1992). The so-collected XRD data should be carefully reduced to atomic PDFs using as precise as possible data for the chemical composition, density, and x-ray absorption factor of the actual sample measured. Simple measures of experimental atomic PDFs quality are described in (Klug and Alexander, 1974; Toby and Egami, 1992; Peterson et al., 2003). Software implementing these measures and correcting experimental atomic PDFs for moderate errors is available as well (Petkov and Danev, 1998). Common problems with the interpretation of atomic PDFs include misidentifying an experimental artifact feature (e.g., a PDF ripple due to the finite Q_{max} value) (Warren and Mozzi, 1975) as a structural feature or vice versa. To avoid such problems, the particular experimental details such as instrument resolution and Q_{max} should be precisely taken into account in the PDF fitting/structure refinement process. Also, structure models resulted from atomic PDFs analysis, in particular when reverse

Monte Carlo simulations are employed, may come out way too disordered, including predicting way too short/long bond lengths and/or way too distorted atomic coordination units unless suitable structure constraints/restraints are imposed on the structure modeling/refinement process. Simple checks for atomic bond lengths and angles feasibility and bond valence sums consistency using available software (Roux and Petkov, 2010) can be done to certify that such mishaps did not occur.

ACKNOWLEDGMENTS

Thanks are due NSF, DOE, NRL, and ICDD for providing funds over several years for atomic PDFs studies, results of which are shown in this paper. Also, thanks are due to Th. Proffen for generating Fig. 2.

LITERATURE CITED

Chupas, P. J., Qiu, X., Hanson, J. C., Lee, P. L., Grey, C. P., and Billinge, S. J. L. 2003. Rapid-acquisition pair distribution function (RA-PDF) analysis. *J. Appl. Cryst.* 36: 1342–47.

Czichos, H., Saito T., and Smith, L. (eds.). 2006. Handbook of Materials Measurements Methods. Springer. Berlin

David, W. I. F., Shakland, K., McCusker, L. B., and Baerlocher, Ch.edts. 2002. Structure Determination from Powder Diffraction. Oxford University Press. Oxford

Egami, T. and Billinge S. J. L. 2003. Underneath the Bragg peaks: Structural Analysis of Complex Materials. Pergamon Press, Elsevier Ltd. New York

Farrow, C. L., Juhás, P., Liu, J. W., Bryndin, D., Božin, E. S., Bloch, J., Proffen, Th., and Billinge, S. J. L. 2007. PDFfit2 and PDFgui: computer programs for studying nanostructure in crystals. *J. Phys.: Condens. Matter* 19: 335219.

Farrow, C. L. and Billinge, S. J. L. 2009. Relationship between the atomic pair distribution function and small-angle scattering: Implications for modeling of nanoparticles. *Acta Cryst. A* 65:232–239.

Farrow, C. L., Shaw, M., Kim, H., Juhas, P., and Billinge, S. J. L. 2011. Nyquist–Shannon sampling theorem applied to refinements of atomic pair distribution functions. *Phys. Rev. B* 84:134105–7.

Gateshki, M., Petkov, V., Pradhan, S. K., and Vogt, T. 2005. Structure of nanocrystalline $MgFe_2O_4$ from x-ray diffraction, Rietveld and atomic pair distribution function analysis *J. Appl. Cryst.* 38:772–79.

Gateshki, M., Niederberger, M., Deshpande, A. S., Ren, Y., and Petkov, V. 2007. Atomic-scale structure of nanocrystalline CeO_2–ZrO_2 oxides by total x-ray diffraction and pair distribution function analysis, *J. Phys.: Condens Matter.*, 19:156205–12.

Gereben, O., Jovari, P., Temleitner, L. and Pusztai, L. 2007. A new version of the RMC++ reverse Monte Carlo programme, aimed at investigating the structure of covalent glasses. *J. Optoelectron. Adv. Mater.* 9:3021–7.

Giacovazzo, C. (ed.). 1998. In Fundamentals of x-ray crystallography. Oxford University Press.

Gilbert, B., Huang, F., Waychunas, G. A., and Banfield, J. F. 2004. Nanoparticles: Strained and stiff. *Science* 305:651–654.

Hahn, T. (ed.). 2002. International Tables for Crystallography. Volume A. Kluwer Academic Publishers. Dordrecht, The Netherlands

Hajdu, F. and Palinkas, G. 1972. On the determination of the absolute intensity of X-rays scattered by a non-crystalline specimen. *J. Appl. Cryst.* 5:395–401.

Jeong, I. K., Proffen, Th., Mohiuddin-Jacobs, F., Billinge, S. J. L. 1999 Measuring correlated atomic motion using X-ray diffraction. *J. Phys. Chem.* 103:921–924.

Juhas, P., Cherba, D. M., Duxbury, P. M., Punch, W. F., and Billinge, S. J. L. 2006. Ab initio determination of solid-state nanostructure. *Nature* 440:655–658.

Keen, D. A. 2001. A comparison of various commonly used correlation functions for describing total scattering. *J. Appl. Cryst.* 34:172–177.

Klug, P. K. and Alexander, L. E. 1974. X-Ray Diffraction Procedures: For Polycrystalline and Amorphous Materials. 2nd ed., John Wiley & Sons, Inc. New York

Kodama, K., Iikibo, S., Taguchi, T., and Shamoto, S. 2006. Finite size effects of nanoparticles on the atomic pair distribution functions. *Acta Cryst.* A 62:444–453.

Kohara, S., Suzuya, K., Kashihara, Y., Matsumoto, N., Umesaki, N., and Sakai, I. 2001. A horizontal two-axis diffractometer for high-energy x-ray diffraction using synchrotron radiation on bending magnet beamline BL04B2 at SPring-8. *Nucl. Instr. and Meth.* A 467–468:1030–33.

Korsunsky, V. I., Neder, B. R., Hofman, A., Dembski, S., Graf, Ch., and Ruhl, E. 2007. Aspects of the modeling of the radial distribution function for small nanoparticles. *J. Appl. Cryst.* 40:975–985.

Kuhs, W. F. and Lehmann, M. S. 1983. The structure of the ice Ih by neutron diffraction. *J. Phys. Chem.* 87: 4312–13.

Lee, J. H., Aydiner, C. C., Almer, J., Bernier, J., Chapman, K. W., Chupas, P. J. Haeffner, D., Kump, K., Lee, P. L., Lienert, U., Miceli, A., and Vera, G. 2008a. Synchrotron applications of an amorphous silicon flat-panel detector. *J. Synchrotr. Rad.* 15:477–488.

Lee, P. L., Shu, D., Ramanathan, M., Preissner, C., Wang, J., Beno, M. A., Von Dreele, R. B. Ribaud, L., Kurtz, Ch., Antao, S. M. Jiao, X., and Toby, B. H. 2008b. A twelve-analyzer detector system for high-resolution powder diffraction. *J. Synchr. Rad.* 15:427–32.

Lindahl, E., Hess, B., and Spoel, D. 2001. GROMACS 3.0: A package for molecular simulation and trajectory analysis. *J. Mol. Modeling*, 7:306–17.

Malenkov, G. 2009. Liquid water and ices: Understanding the structure and physical properties. *J. Phys.: Condens. Matter.* 21:283101–35.

Midgley, P. A. and Dunin-Borkowski, R. E. 2009. Electron tomography and holography in materials science. *Nat. Mat.* 8:271–280.

Mullen, K. and Levin, I. 2011. Mitigation of errors in pair distribution function analysis of nanoparticles. *J. Appl. Cryst.* 44:788–97.

Neder, R. B. and Proffen, Th. 2008. Diffuse scattering and defect structure simulations. A Cook Book using the Program DISCUS. Oxford University Press. Oxford

Page, Y. Le and Donnay, G. 1976. Refinement of the crystal structure of low-quartz. *Acta Cryst.* 32:2456–2459.

Peterson, P. F., Bozin, E. S., Proffen, Th., and Billinge, S. J. L. 2003. Improved measures of quality of atomic pair distribution function quality. *J. Appl. Cryst.* 36:53–64.

Petkov, V. and Danev, R. 1998. IFO—a program for image reconstruction-type calculation of atomic distribution functions for disordered materials. *J. Appl. Cryst.* 31:609–19.

Petkov, V., Jeong, I-K., Chung, J. S., Thorpe, M. F., Kycia, S. and Billinge S. J. L. 1999. High-real space resolution measurement of the local structure of $In_xGa_{1-x}As$ semiconductor alloys using X-ray diffraction. *Phys. Rev. Lett.* 83:4089–92.

Petkov, V., Billinge, S. J. L., Sashtri, S., and Himmel, B. 2000. Polyhedral units and connectivity in calcium aluminosilicate glasses from high-energy x-ray diffraction. *Phys. Rev. Lett.* 85:3436–9.

Petkov, V., Billinge, S. J. L., Larson, P., Mahanti, S. D., Vogt, T., Rangan, K. K., and Kanatzidis, M. 2002. Structure of nanocrystalline materials using atomic pair distribution function analysis: Study of $LiMoS_2$ *Phys. Rev. B.* 65: 092105.

Petkov, V., Peng, Y., Williams, G., Huang, B., Tomalia, D., and Ren, Y. 2005a. Structure of gold nanoparticles suspended in water studied by x-ray diffraction and computer simulations, *Phys. Rev. B* 72:195402–8.

Petkov, V., Parvanov, V., Tomalia, D., Swanson, D., Bergstrom, D., and Vogt, T. 2005b. 3D structure of dendritic and hyper--branched macromolecules by x-ray diffraction", *Solid State Commun.* 134*:* 671–75.

Petkov, V. 2008 Nanostructure by high-energy XRD. *Mater. Today* 11:28–38.

Petkov, V., Cozzoli, P. D., Buonsanti, R., Cingolani, R., and Ren, Y. 2009. Size, shape and internal atomic ordering of nanocrystals by atomic pair distribution functions: a comparative study of gamma-Fe_3O_3 nanosized spheres and tetrapods. *J. Am. Chem. Soc.* 131:14264–6.

Petkov, V. and Shastri, S. 2010. Element-specific view of the atomic ordering in materials of limited structural coherence by high-energy resonant x-ray diffraction and atomic pair distribution functions analysis: A study of PtPd nanosized catalysts. *Phys. Rev. B* 81:165428.

Petkov, V., Selbach, S. M., Einarsrud, M.-A., Grande, T., and Shastri, S. D. 2010a. Melting of Bi-sublattice in nanosized $BiFeO_3$ perovskite by resonant x-ray diffraction. *Phys. Rev. Lett.* 105:185501–4.

Petkov, V., Moreels, I., Hens, Z., and Ren, Y. 2010b. PbSe quantum dots: Finite, off-stoichiometric, and structurally distorted. *Phys. Rev. B* 81:241304–4.

Petkov, V. and Messurier, D. Le. 2010. Atomic-scale structure of $GeSe_2$ glass revisited: a continuous or broken network of Ge-$(Se_{1/2})_4$ tetrahedra. *J. Phys.: Condens. Matter* 22: 115402–6.

Pradhan, S. K., Deng, Z. T., Tang, F., Wang, C., Ren, Y., Moeck, P., and Petkov, V. 2007. 3D structure of CdX (X = Se, Te) nanocrystals by total x-ray diffraction. *J. Appl. Phys.* 102:044304–7.

Qiu, X., Thompson, J. W., and Billinge, S. J. L. 2004a. PDFgetX2: A GUI driven program to obtain the pair distribution function from X-ray powder diffraction data. *J. Appl. Cryst.* 37:678–78.

Qiu, X., Bozin, E. S., Juhas, P., Proffen, Th., and Billinge, S. J. L. 2004b. Reciprocal-space instrumental effects on the real-space neutron atomic pair distribution function. *J. Appl. Cryst.* 37:110–16.

Roux, S. Le, Martin, S., Christensen, R., Ren, Y., and Petkov, V. 2011. Three dimensional structure of multicomponent $(Na_2O)_{0.35}$ $[(P_2O_5)_{1-x}$ $(B_2O_3)_x]_{0.65}$ glasses by high energy X-ray diffraction and constrained reverse Monte Carlo simulations. *J. Phys.: Condens. Matter* 23:035403.

Roux, S. Le and Petkov, V. 2010. ISAACS—Interactive structure analysis of amorphous and crystalline systems. *J. Appl. Crystallogr.* 43:181–85.

Ruland, W. 1964. The separation of coherent and incoherent Compton x-ray scattering. *Brit. J. Appl. Phys.* 15: 1301–07.

Samy, A. Dinnebier, R. E. Smaalen, S. Van 2010. Maximum entropy method and charge flipping, a powerful combination to visualize the true nature of structural disorder from in situ x-ray powder diffraction data. *Acta Cryst. B* 66: 184–195.

Smith, D. K. and Jenkins, R. 1996. The powder diffraction file: Past, present, and future. *J. Res. Natl. Inst. Stand. Technol.* 101:259–271.

Soper, A. K. and Barney, E. R. 2011. Extracting the pair distribution function from white-beam X-ray total scattering data. *J. Appl. Cryst.* 44:714–26.

Thijsse, B. J. 1984. The accuracy of experimental radial distribution functions for metallic glasses. *J. Appl. Cryst.* 17:61–76.

Toby, B. H. and Egami, T. 1992. Accuracy of pair distribution function analysis applied to crystalline and non-crystalline materials. *Acta Cryst. A* 48:336–346.

Warren, B. E. 1934 The diffraction of X-rays in glass. *Phys. Rev. B.* 45:657–661.

Warren, B. E. and Mozzi, R. L. 1975. The termination effect for amorphous patterns. *J. Appl. Cryst.* 8:674–677.

Wagner, C. N. J. 1969. Structure of amorphous alloy films. *J. Vac. Sci. Tech.* 6:650–657.

Zachariasen, W. H. 1932. The atomic arrangement in glass. *J. Am. Chem. Soc.* 54:3841–3851.

KEY REFERENCES

Egami and Billinge, 2003. See above.

This book is an excellent summary of the atomic PDFs analysis and its application to crystals with intrinsic disorder.

Keen, 2001. See above.

This paper gives an overview of the various definitions of atomic PDFs used by the scientific community.

Klug and Alexander, 1974. See above

This book presents a detailed explanation of the principles of traditional powder XRD and its extension into atomic PDFs analysis.

Thijsse, 1984. See above.

This article provides a detailed account of XRD experiments aimed at atomic PDFs analysis.

Wagner, 1969. See above.

The paper introduces the most frequently used atomic PDF definition.